JOURNAL OF SPACECRAFT AND ROCKETS
Vol. 35, No. 4, July–August 1998

Analytic Corrections to Computational Heating Predictions Accounting for Changes in Surface Catalysis

Peter A. Gnoffo*
NASA Langley Research Center, Hampton, Virginia 23681-0001
and
George R. Inger†
Iowa State University, Ames, Iowa 50011-3231

A new approach for combining the insight afforded by integral boundary-layer analysis with comprehensive (but time-intensive) computational fluid dynamic flowfield solutions of the thin-layer Navier–Stokes equations is described. The approach extracts computationally simulated quantities at the wall and at the boundary-layer edge for inclusion in a postprocessing boundary-layer analysis. It allows a designer at a workstation to address the question, given a single computational solution, "How much does the heating change for a thermal protection system with catalytic properties different from those used in the original numerical simulation?" Capabilities of this approach for application to reusable launch vehicle design are demonstrated. If the definition of surface catalysis is uncertain early in the design process, results show that fully catalytic wall boundary conditions provide the best baseline for computationally simulated design points.

Nomenclature

C_D = equilibrium constant, $p_e e^{\theta_D}[\alpha_e^2/(1-\alpha_e^2)]_{\text{eq}}$
$\hat{C}_p$ = specific heat of molecules, J/kmole-K
h = enthalpy per unit mass of mixture, J/kg
h_D = heat of formation per unit mass of species, J/kg
$I_{(1-3,D)}$ = reaction integrals
k_r = recombination rate coefficient, m^6/kmole^2-s
Le = Lewis number
Pr = Prandtl number
p = pressure, N/m^2
Q = heat transfer function
q = surface heating, W/m^2
R = radius of curvature, m
R_s = gas constant for species s, J/kg-K
R_u = universal gas constant, 8314.3 J/kmole-K
r = ratio of velocity gradients
Sc = Schmidt number
T = temperature, K
T_D = characteristic temperature of dissociation, K
u, w = streamwise and crossflow velocities, m/s
V = total velocity, m/s
x, z = streamwise and crossflow distances, m
Z = bridging function
α = mass fraction of atoms
Γ^* = composite Dahmkohler number
$\Gamma_c, \tilde{\Gamma}_c$ = Dahmkohler numbers for surface catalysis
Γ_D = Dahmkohler number for dissociation dominated flow
Γ_G = Dahmkohler number for recombination dominated flow
γ = catalytic efficiency of surface
θ = temperature ratio T/T_e
θ_D = temperature ratio T_D/T_e
μ = viscosity, N-s/m^2
ξ, η = Levy–Lees transformation coordinates
ρ = density, kg/m^3
χ = parameter $u_e(\mathrm{d}\xi/\mathrm{d}x)(1+r)/\xi$, 1/s

Subscripts

e = boundary-layer edge
eq = equilibrium
F = frozen
i, j = computational fluid dynamics mesh point location
N = nitrogen atom
O = oxygen atom
w = wall
γ = computed using γ equals $\gamma(T)$
0 = computed using γ equals 0
1 = computed using γ equals 1
∞ = freestream

Received Aug. 22, 1997; revision received Feb. 7, 1998; accepted for publication Feb. 12, 1998.

*Aerospace Engineer, Aerothermodynamics Branch, Aero- and Gas-Dynamics Division. Associate Fellow AIAA.
†Professor, Department of Aerospace Engineering and Engineering Mechanics. Associate Fellow AIAA.

Introduction

THE grand challenge of computational fluid dynamics (CFD) is to produce accurate solutions on real configurations in a matter of minutes. However, the reality of CFD simulation today is that computational expense and the complexity of surface definition and grid generation restrict the number of cases that can be produced. Given this limitation, a challenge often overlooked by the CFD community concerns the timely transmission and efficient utilization of the CFD solution(s) by all members of a vehicle design team. Recent experiences with the phase I design process for the X33 have revealed opportunities for development of software to better exploit a limited CFD solution matrix. Extraction of only a few parameters at the surface and at the boundary-layer edge of a CFD solution can enable analytic extension of heat transfer solutions beyond the baseline matrix.

Integral boundary-layer solution techniques applicable to the problem of determining aerodynamic heating rates of hypersonic vehicles in the vicinity of stagnation points, windward centerlines, and swept-wing leading edges are discussed in the literature.[1–4] The analyses include effects of finite-rate gas chemistry across the boundary layer and finite-rate catalysis of atom recombination at the surface. A new approach for combining the insight afforded by integral boundary-layer analysis with comprehensive (but time-intensive) CFD flowfield solutions of the thin-layer Navier–Stokes equations is described. The approach extracts CFD-derived quantities at the wall and at the boundary-layer edge for inclusion in a postprocessing boundary-layer analysis. The postprocessed database allows a designer at a workstation, given a single CFD solution, to

determine how the heating changes as a function of changes in the choice of a thermal protection system. Changes in both surface recombination rate and emissivity can be accommodated. For a given trajectory point, the approach uses a single CFD solution obtained with a known variation of catalytic efficiency over the vehicle surface. Changes to CFD baseline heating levels are calculated as a function of changes in catalytic efficiency derived from integral boundary-layer solution techniques that utilize CFD-generated edge and wall conditions.

The present paper reviews and extends work presented in an earlier report.[5] A reformulation of the algorithm designated method 1G, with continuous change of catalysis, generalized validity,[5] is developed that better models the different roles of oxygen and nitrogen chemistry across the boundary layer and at the wall. The test cases focus on flow over a sphere at several trajectory points characteristic of re-entry of a representative winged single-stage-to-orbit vehicle. CFD calculations are made for three wall catalysis models at each of these points. The models include noncatalytic, finite catalytic (Shuttle tile), and fully catalytic wall boundary conditions. The postprocessed integral boundary-layer corrections using each of three baseline CFD heating results are compared to actual CFD calculations for the corresponding off-baseline case. The results of tests using the same reformulation of method 1G on vehicles of realistic geometric complexity appropriate for a reusable launch vehicle (RLV) are presented. Relative differences in predicted heating levels between single CFD runs with postprocessed corrections and multiple CFD runs using different wall catalysis models are discussed.

An integral solution approach to an important, related problem, i.e., heating spikes across the interface of two surfaces with different catalytic efficiencies, was also introduced in the earlier report.[5] That analysis showed that the integral method properly bounded the larger-scale accommodation but missed some elements of the upstream influence and near-juncture behavior. A more comprehensive analysis is currently being tested to address this issue but is not discussed here.

The goal of this research is to create a stand-alone postprocessing tool that can be used in preliminary design of thermal protection systems (TPS) for hypersonic vehicles. The tool would make extensive use of a small number of CFD solutions computed using a relatively simple surface catalysis model. Design iterations are conducted without the need for additional CFD runs until convergence on a single concept is achieved, at which point CFD should be used to provide a final check and/or recalibration point.

Baseline CFD Solution Algorithm

The CFD baseline solutions for real gas, viscous analysis are provided by LAURA.[6–8] Comparisons to experimental data for hypersonic flows in air are documented in the literature.[9–13] The code employs upwind-biased, point-implicit relaxation. Inviscid fluxes are approximated with Roe's averaging,[14] eigenvalue limiting (similar to that of Harten[15]), and Yee's[16] symmetric total variation diminishing scheme. Viscous fluxes are approximated with central differences. A model for surface catalytic efficiency[17] $\gamma(T)$ used in the present work is defined by

$$\begin{aligned}
\gamma_O &= 40e^{-11440/T_w}, && 1435 < T_w < 1580 \\
\gamma_O &= 39.9\,10^{-9}e^{21,410/T_w}, && 1580 < T_w < 1845 \\
\gamma_N &= 0.061e^{-2480/T_w}, && 1410 < T_w < 1640 \\
\gamma_N &= 0.00061e^{5090/T_w}, && 1640 < T_w < 1905
\end{aligned} \tag{1}$$

(A more recent compilation of catalytic efficiencies[18] is now available that gives rates somewhat different from those of the present study.) The catalytic recombination rate $K_{w,s}$ for species s is then defined by

$$K_{w,s} = \gamma_s(T_w)\sqrt{R_s T_w/2\pi} \tag{2}$$

Integral Boundary-Layer Method

Highlights

Integral boundary-layer theory for evaluating nonequilibrium effects on surface heating has been described previously.[2–4] Key features of the analysis are reviewed here. First, the model accounts for both finite catalysis of the surface and finite reactivity of the boundary layer. The finite catalysis of the surface enters the analysis through the Dahmkohler number Γ_c, the ratio of atom recombination time at the surface and a characteristic local diffusion time,

$$\Gamma_c = (\rho_w/\mu_w\chi)^{\frac{1}{2}} Sc K_w \tag{3}$$

The finite reactivity of the boundary layer enters the analysis through the Dahmkohler number Γ_G and Γ_D, the ratio of characteristic local flow time to gas phase reaction time. In the case of recombination-dominated boundary layers (near stagnation points),

$$\Gamma_G = \frac{2k_r T_e^{-2} p_e^2}{R_u^2 \chi} \tag{4}$$

In the case of dissociation-dominated boundary layers (near windside centerline at low angles of attack, where viscous shear raises temperatures in the boundary layer),

$$\Gamma_D = (C_D/p_e)\Gamma_G \tag{5}$$

Second, analytic solutions to the governing boundary-layer equations can be made with simplifying approximations in the vicinity of the vehicle stagnation point (nose region), swept leading-edge region, and windward centerline region. The parameter χ

$$\chi = u_e\left(\frac{\mathrm{d}\xi}{\mathrm{d}x}\right)\frac{1+r}{2\xi} \tag{6}$$

is a function of the Levy–Lees transformed coordinate ξ and takes on relatively simple, limiting values in these regions. The Levy–Lees transformed coordinate is defined by

$$\xi = \int_0^x \rho_w \mu_w u_e \,\mathrm{d}x \tag{7}$$

Three-dimensional effects are included with the parameter $1+r$, where r is the ratio of velocity gradients at the edge of the boundary layer:

$$r = \left(\frac{\mathrm{d}w_e}{\mathrm{d}z}\right)\Big/\left(\frac{\mathrm{d}u_e}{\mathrm{d}x}\right) \tag{8}$$

The postprocessing algorithm used to correct for changes in surface heating associated with global change of the surface catalysis model over a hypersonic vehicle is denoted method 1. The initial formulation of method 1 (Ref. 5) was restricted to the nose region because of the need to utilize a simple, analytic relation for χ. Subsequent modifications denoted method 1G, which are more generally applicable to the complete vehicle surface, are presented here.

Global Change of Catalysis: Method 1G

Surface heating beneath a recombination-dominated boundary layer can be expressed[2] as an appropriate interpolation of an equilibrium boundary-layer heating rate $Q_{w,\mathrm{eq}}$ and a frozen boundary-layer heating rate $Q_{w,F}$ by

$$Q_w = Q_{w,\mathrm{eq}} + Z(\Gamma^*)(Q_{w,F} - Q_{w,\mathrm{eq}}) \tag{9}$$

In Eq. (9) the variable Q is a dimensionless heating rate, related to the dimensional heating rate q_w by

$$Q_w = q_w \frac{-Pr/\hat{C}_p T_e}{\sqrt{\rho_w \mu_w \chi}} \tag{10}$$

The equilibrium boundary-layer heating rate $Q_{w,\mathrm{eq}}$ reference value at each mesh point (i, j) on a discretized vehicle surface is defined[2] by

$$Q_{w,\mathrm{eq},i,j} = 0.47 Pr_{w,i,j}^{-\frac{2}{3}}\left(1 - \theta_w + \sqrt{Pr_w}\frac{u_e^2}{2\hat{C}_p T_e} + Le_w^{0.52}\frac{\alpha_e h_D}{\hat{C}_p T_e}\right)_{i,j} \tag{11}$$

The reference value for frozen boundary-layer heating rate $Q_{w,F}$ at each mesh point (i, j) is defined[19] by

$$Q_{w,F,i,j} = 0.47 Pr_{w,i,j}^{\frac{1}{3}} \times \left(1 - \theta_w + \sqrt{Pr_w}\frac{u_e^2}{2\hat{C}_p T_e} + Le_w^{0.67}\frac{\alpha_e h_D}{\hat{C}_p T_e}\frac{\tilde{\Gamma}_c}{1+\tilde{\Gamma}_c}\right)_{i,j} \quad (12)$$

Equation (12) accounts for finite surface catalysis through the Dahmkohler number $\tilde{\Gamma}_{c,i,j} \equiv \Gamma_{c,i,j}/(0.47 Sc^{1/3})$ but does not include effects of reactions across the boundary layer.

The bridging function $Z(\Gamma^*)$ in Eq. (9) varies from 0 (equilibrium limit with three-body recombination rates much faster than local flow rates) to 1 (frozen limit with three-body recombination rates much slower than local flow rates). It is derived from a fundamentally based analysis of the atomic species conservation equations and is given by

$$Z(\Gamma^*) \approx \frac{3\sqrt{1 + 16\Gamma^*_{i,j}/9} - 1}{2 + 4\Gamma^*_{i,j}} \quad (13)$$

where $\Gamma^*_{i,j}$ is a composite Dahmkohler number defined at each surface mesh point by

$$\Gamma^*_{i,j} = \alpha_{e,i,j}\left[\frac{I_1 + 2\tilde{\Gamma}_c I_2 + \tilde{\Gamma}_c^2 I_3}{(1+\tilde{\Gamma}_c)^2}\right]_{i,j}\Gamma_{G,i,j} \quad (14)$$

The integrals I_1, I_2, and I_3 account for integrated effects of reactions across the boundary layer on heating rates. They are tabulated[3] and curve fits are provided:

$$I_1 \approx 4.80(0.50/Sc_w)^{0.45}\theta_w^{0.80(1-\omega)-1.84}$$
$$I_2 \approx 1.80(0.50/Sc_w)^{0.12}\theta_w^{0.63(1-\omega)-1.15} \quad (15)$$
$$I_3 \approx 0.93(0.50/Sc_w)^{-0.22}\theta_w^{0.41(1-\omega)-0.65}$$

These integral approximations are valid over a parameter range $0.04 \le \theta_w \le 0.50$ and $-2 \le \omega \le 0$.

In the test problems considered here, the bridging function for oxygen recombination Z_O is based on a recombination rate $k_{r,O} = 7.8510^{13} T^{\omega}$ with $\omega = -1.5$. This rate constant was used in earlier work.[3] Other numerical experiments[5] using a recombination rate extracted from Park's kinetic model yielded equivalent results for Z_O. Recombination rates for atomic nitrogen are approximately 1–100 times faster than for atomic oxygen, the factor depending on collision partner and temperature. These rates yield values for Z_N of approximately 1 in the test problems, indicating frozen flow. However, inspection of the near wall atom profiles from the CFD baseline solutions show nitrogen recombination far in excess of that predicted by frozen flow. The approximations in the integral boundary-layer theory do not account for two-body, exothermic reactions that deplete atomic nitrogen through collisions with molecular oxygen to form NO and O and through collisions with nitric oxide to form N_2 and O. Consequently, the bridging function for nitrogen recombination Z_N was based on an effective rate coefficient $k_{r,N} = 2000 k_{r,O}$ that approximately calibrates the depletion of atomic nitrogen approaching the wall in a manner consistent with CFD results. The calibration has not been tested outside the test matrix discussed in a later section.

Additional approximations have been employed in method 1G to simplify extraction of CFD-derived quantities. In extracting CFD baseline quantities, the boundary-layer edge is defined as the point where total enthalpy equals 0.995 of total freestream enthalpy. Velocity at the boundary-layer edge is taken as the component that is parallel to the surface. Because energy is used as a primary variable and temperature is a derived quantity in the CFD analysis, $h - \alpha h_D$ is substituted for $C_p T$, where

$$\alpha h_D = \sum_s \alpha_s h_{D,s}$$

and $(h - \alpha h_D)/(h - \alpha h_D)_e$ is substituted for θ in the preceding equations. To model the catalytic effect of the surface on homogeneous recombination of both nitrogen and oxygen atoms, Eq. (9) is modified as follows:

$$Q_{w,i,j} = Q_{w,eq,i,j} + 0.47 Pr_{w,i,j}^{\frac{1}{3}} \times \left[Z_O\frac{\alpha_{O,e} h_{D,O}}{\hat{C}_p T_e}\left(Le_w^{0.67}\frac{\tilde{\Gamma}_{c,O}}{1+\tilde{\Gamma}_{c,O}} - Le_w^{0.52}\right) + Z_N\frac{\alpha_{N,e} h_{D,N}}{\hat{C}_p T_e}\left(Le_w^{0.67}\frac{\tilde{\Gamma}_{c,N}}{1+\tilde{\Gamma}_{c,N}} - Le_w^{0.52}\right)\right]_{i,j} \quad (16)$$

The Dahmkohler numbers in Eqs. (3–5) and the dimensional heating in Eq. (10) require evaluation of the rate parameter χ. Parameter χ is itself a function of the boundary-layer coordinate ξ [Eq. (7)] and a local flow dimensionality parameter r [Eq. (8)]. Analytic approximations to these parameters are available in special regions,[2] e.g., stagnation point, windside centerline, and swept wing leading edge. However, direct evaluation of the boundary-layer coordinate ξ through Eq. (7) is a tedious process on a realistic configuration, requiring streamline tracing back to the original attachment point(s). A simpler approach is to solve for the value of χ, which yields q_w using boundary-layer edge and wall properties from the baseline CFD solution. The CFD values of q_w implicitly contain the streamline history and local flow dimensionality effects. A Newton iteration works quite efficiently to handle the nonlinear functionality of q_w on χ. This same value of χ is then used in the integral boundary-layer formulation for the new values of catalysis (and wall temperature, if required) to compute the new heating distribution. The approximation for χ ignores integrated effects of changes in surface temperature and density along the surface streamline but works well in limited tests performed to date.

The Lewis number may be evaluated in a variety of ways, reflecting the uncertainty of modeling multicomponent diffusion with a single parameter in the integral boundary-layer theory. It has been calculated based on the diffusivity of atomic oxygen diffusing in molecular nitrogen and on a number density weighted average of the diffusion coefficients for each species as computed in the CFD algorithm. The weighted averages can be defined to reflect new (predicted) mass fractions at the surface. There is no single formulation that has been found to be consistently better than any other in the matrix of test problems considered here. Consequently, the simplest approach, which is to extract the Lewis number directly from the CFD solution, has been employed in the results that follow.

In the most general case with high Mach numbers at the boundary-layer edge, viscous dissipation of kinetic energy tends to produce a local maximum temperature within the boundary layer. The higher temperature may lead to dissociation-dominated chemistry within the boundary layer. Inclusion of this effect leads to the following correction, which may be added to Eq. (12) or Eq. (16):

$$\Delta Q_{w,F} = -0.47 Pr_w^{\frac{1}{3}}\Gamma_D I_D\frac{h_D}{\hat{C}_p T_e}\left[1 - \frac{Le_w\tilde{\Gamma}_c}{1+\tilde{\Gamma}_c}\right] \quad (17)$$

where I_D is a reaction integral, discussed and tabulated by Inger.[2]

Test Cases

Sphere

Tests of method 1G for hypersonic flow over a 0.6-m-radius sphere are presented. Surface heating rates are computed for three different wall catalytic boundary conditions at trajectory points defined in Table 1. The wall temperature in each case is defined by a radiative equilibrium wall boundary condition with emissivity $\epsilon = 0.9$. Grid resolution is 30 cells in the streamwise direction and 64 cells

Table 1 Trajectory and heating

Point	V_∞, m/s	ρ_∞, kg/m^3	T_∞, K	q_1, W/cm^2	q_γ, W/cm^2	q_0, W/cm^2
1	5493	2.00^{-4}	238	52.1	41.4	25.2
2	4440	3.53^{-4}	250	34.6	30.4	20.5
3	3551	6.64^{-4}	264	21.8	18.6	14.7

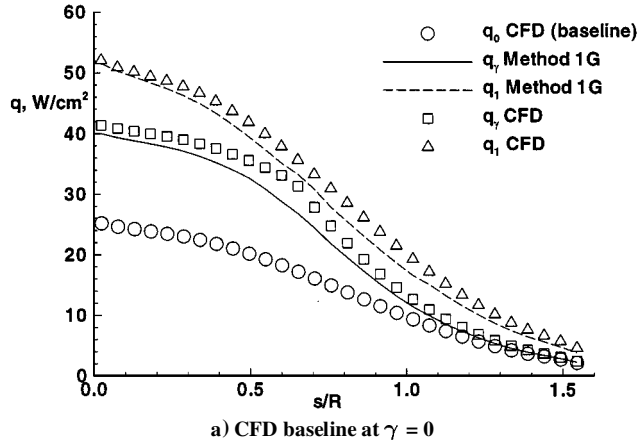

a) CFD baseline at $\gamma = 0$

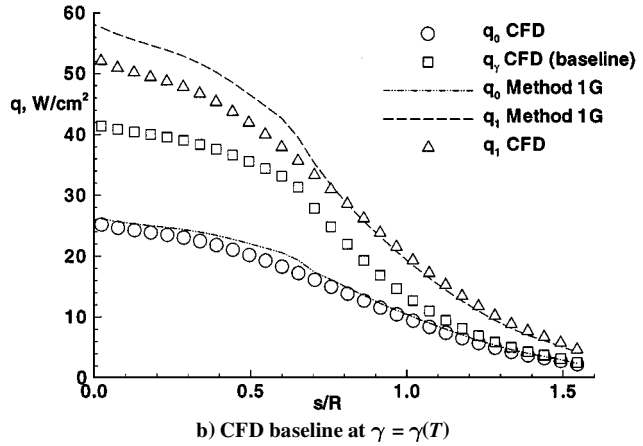

b) CFD baseline at $\gamma = \gamma(T)$

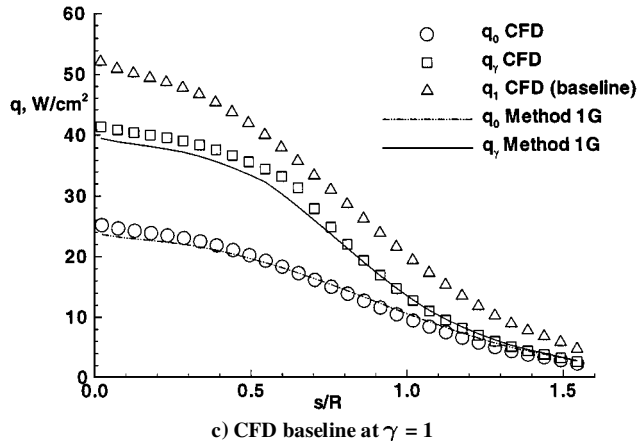

c) CFD baseline at $\gamma = 1$

Fig. 1 Comparison of CFD heating levels (symbols) with method 1G corrections (lines) derived from CFD baseline for point 1 as function of three surface catalysis models.

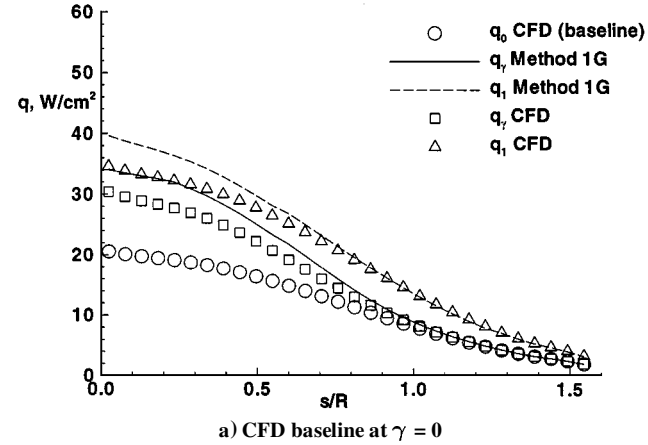

a) CFD baseline at $\gamma = 0$

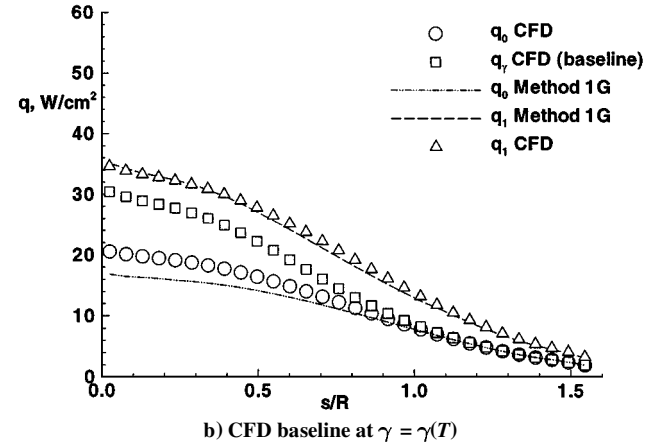

b) CFD baseline at $\gamma = \gamma(T)$

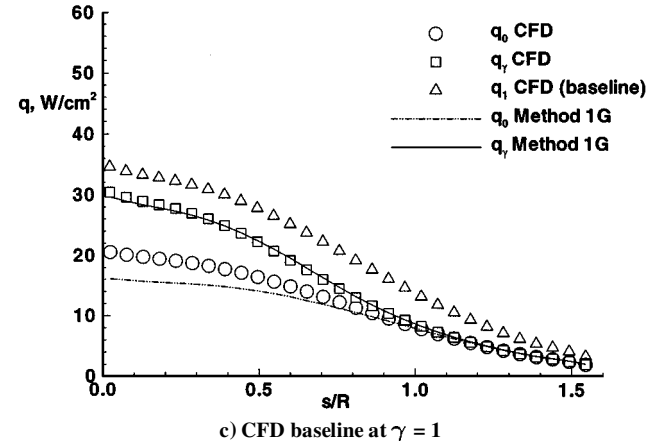

c) CFD baseline at $\gamma = 1$

Fig. 2 Comparison of CFD heating levels (symbols) with method 1G corrections (lines) derived from CFD baseline for point 2 as function of three surface catalysis models.

across the shock layer. The cell Reynolds number at the wall in all cases is less than 6. These results differ from those presented earlier[5] in that the current methodology is not restricted to the nose region and the CFD results were all run at their respective radiative equilibrium wall temperatures. A secondary iteration was employed in method 1G to accommodate the implicit, functional dependence of Γ_c and θ_w on the wall temperature.

In Fig. 1a, the noncatalytic solution is treated as the available CFD baseline solution. This baseline CFD data set has been postprocessed using method 1G to obtain corrected heating levels associated with changes in the surface catalysis model to finite catalytic and to fully catalytic. The actual CFD heating predictions with the new surface catalysis models are compared with the results of method 1G in Fig. 1a.

Similar comparisons are made in Fig. 1b for point 1 except that the finite catalytic CFD solution is used as a baseline and postprocessed corrections are derived for the fully catalytic and noncatalytic surfaces. The fully catalytic CFD solution is used as a baseline in Fig. 1c. Comparisons of method 1G with CFD at successive trajectory points are presented in Fig. 2 for point 2 and Fig. 3 for point 3.

Surface catalysis plays a major role in the stagnation region heating rate in all of the test problems. Method 1G predicts that roughly 56% of the total heating at point 1 is associated with diffusion of atoms that recombine at the surface of a fully catalytic wall. In this specific case, approximately 26% of the fully catalytic heating result is associated with diffusion of oxygen atoms to the surface and another 30% with the diffusion of nitrogen atoms to the surface. At point 2, approximately 40% of the fully catalytic heating result is associated with diffusion of oxygen atoms to the surface and less than 1% with the diffusion of nitrogen atoms to the surface. At point 3, approximately 33% of the fully catalytic heating result is

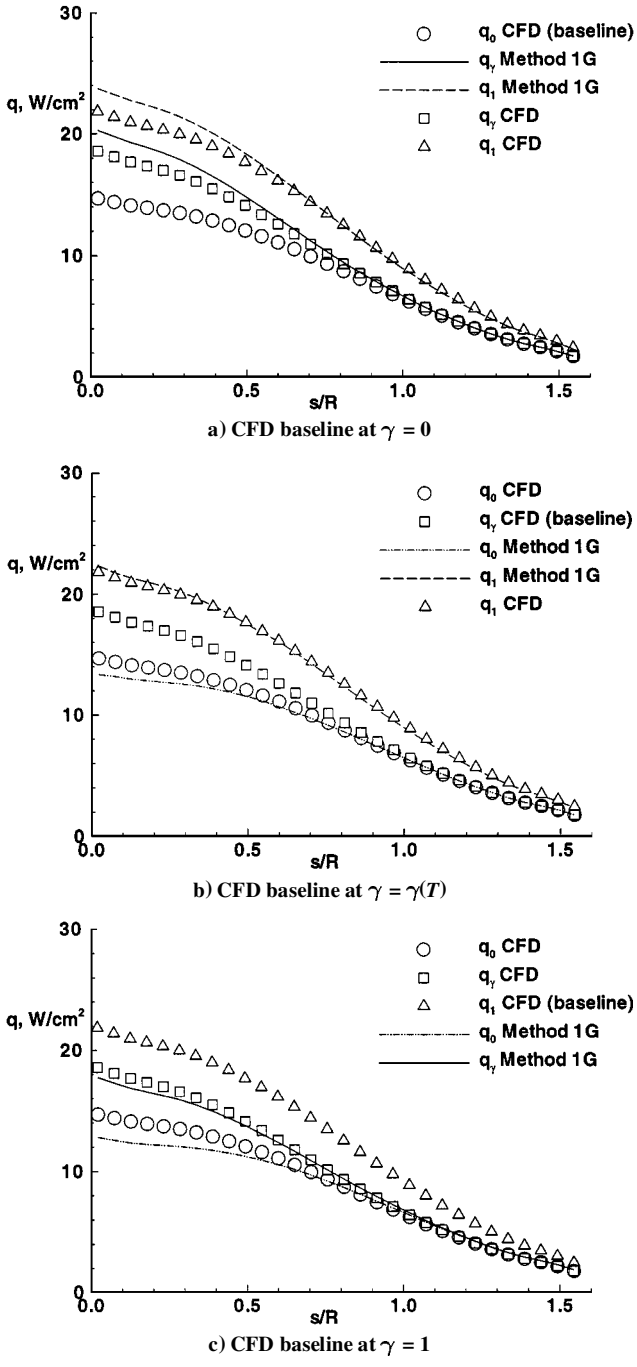

Fig. 3 Comparison of CFD heating levels (symbols) with method 1G corrections (lines) derived from CFD baseline for point 3 as function of three surface catalysis models.

associated with diffusion of oxygen atoms to the surface and nearly 0% with the diffusion of nitrogen atoms to the surface. The contribution of nitrogen atoms rapidly diminishes as flow expands around the sphere at point 1 because the mass fraction of atomic nitrogen at the boundary-layer edge goes to zero.

Initial predictions for $\alpha_{N,w}$ at point 1 using a conventional value for $k_{r,N}$ in Eq. (4) were much larger than CFD results. As noted earlier, the approximations in the integral boundary-layer theory do not account for two-body, exothermic reactions that deplete atomic nitrogen through collisions with molecular oxygen to form NO and O and through collisions with nitric oxide to form N_2 and O. These reaction mechanisms also help explain why method 1G predictions for atomic oxygen near the surface tend to underpredict (5–20%) the CFD results when atomic nitrogen exists at the boundary-layer edge. Increasing the value of the effective nitrogen recombination rate coefficient ($k_{r,N} = 2000k_{r,O}$) approximately models the depletion of atomic nitrogen approaching the wall in a manner consistent with CFD results.

The large changes in surface heating associated with changes in surface catalysis models are generally well predicted across the test matrix. Nitrogen chemistry plays a major role in the stagnation region at the first trajectory point. Oxygen chemistry is the predominant factor away from the stagnation point and at the stagnation point later in the trajectory. Method 1G predictions are within 7% of CFD results away from the stagnation point ($s/R > 0.8$) in all but one case. The exception, a point 1 prediction of fully catalytic heating based on a noncatalytic CFD baseline, is within 12% of the CFD result. Stagnation region heating predictions by method 1G at point 3, where nitrogen chemistry is not important, are within 10% of CFD results in all but one case. The exception here is for the prediction of noncatalytic heating from a fully catalytic CFD baseline, which is within 17% of the CFD result. Stagnation region heating predictions for the first two trajectory points in which nitrogen chemistry begins to play an important role are within 20% of the CFD results.

Application of method 1G to real design problems is unlikely to involve noncatalytic boundary conditions. Noncatalytic surface specification in the CFD analysis is insufficiently conservative for TPS design purposes, even in cases where low catalytic coatings are used, e.g., Shuttle tiles. In cases where nitrogen chemistry plays an active role, it is evident in Figs. 1 and 2 that even a little surface catalysis can produce heating levels that are closer to being fully catalytic than noncatalytic. In all cases where method 1G is used to calculate fully catalytic heating from a finite catalytic baseline CFD solution, the resultant prediction is within 12% of the CFD result. In all cases where method 1G is used to calculate finite catalytic heating from a fully catalytic baseline CFD solution, the resultant prediction is within 5% of the CFD result. Consequently, it is advised that fully catalytic baseline CFD solutions be run early in the design phase of a hypersonic vehicle. This approach yields CFD solutions for laminar, nonequilibrium flows that 1) are conservative, 2) converge more quickly than with finite catalytic or noncatalytic surface conditions, and 3) provide the best baseline for analytic extrapolation to various TPS design options.

RLV

Application of method 1G to a relatively complex configuration is tested. The front and midsections of an RLV candidate configuration (Fig. 4) for a flowfield simulation at Mach 25, 45-deg angle of attack, and 79.6-km altitude are examined. The surface grid representation for the front section is defined with 52 streamwise cells and 64 circumferential cells. The surface grid representation for the midsection is defined with 18 streamwise cells and 77 circumferential cells. The shock layer is resolved with 64 cells. Heating rates for both a fully catalytic wall and a finite catalytic wall were computed at the respective radiative equilibrium wall temperatures. A secondary iteration was employed in method 1G to accommodate the implicit, functional dependence of Γ_c and θ_w on the wall temperature.

Circumferential heating distributions as a function of computational coordinate j varying from leeside ($j = 1$) to windside ($j = 64$) are presented in Fig. 5a for the front section. The circumferential cut is from the $i = 40$ plane, which lies far downstream from the nose and upstream of a wing. The windside centerline heating distribution as a function of computational coordinate i varying from the stagnation point ($i = 16$) to the exit plane of the front section

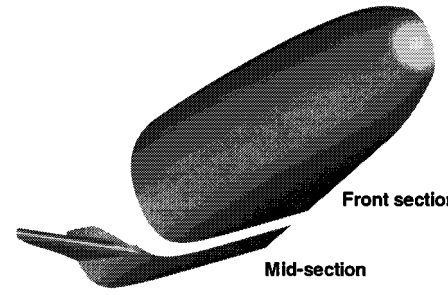

Fig. 4 Front and midsections of RLV test configuration.

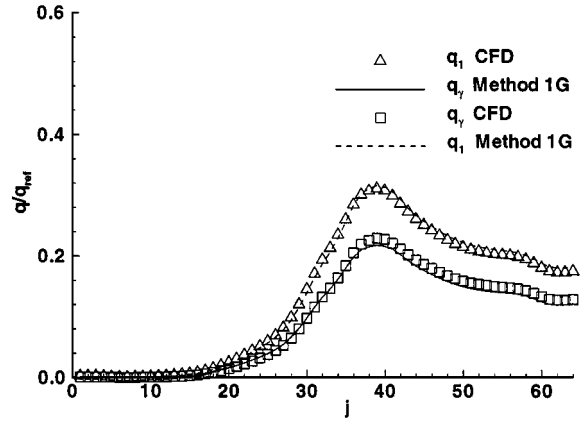

a) Circumferential distribution, $i = 40$

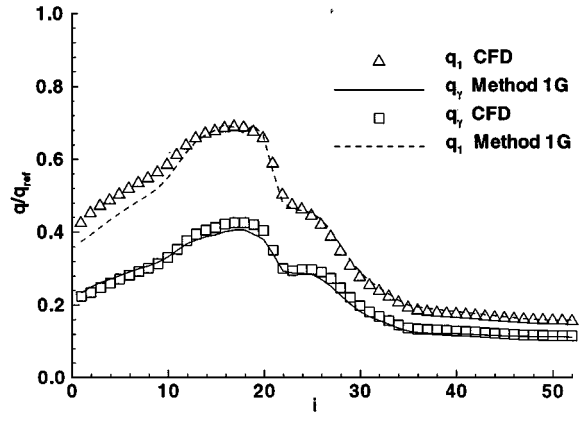

b) Centerline distribution, $j = 64$

Fig. 5 Comparison of CFD heating levels obtained on front section of RLV with method 1G predictions obtained at $\gamma = \gamma(T)$ and 1 at Mach 25 and 79.6 km.

($i = 52$) is presented in Fig. 5b. Method 1G corrections to CFD baseline heating are generally within 5% of computations. In the earlier version of method 1G (Ref. 5), a separate bridging function for nitrogen Z_N was not used, and comparisons in the stagnation region were only within 20%.

The midsection of the RLV (Fig. 4) includes the windside surface, the wing, and a small part of the leeside surface. The CFD and integral-boundary-layer results for heating on this section are compared in Fig. 6. Comparisons are generally within 5% in a circumferential direction around the wing leading edge (Fig. 6a), around the windside surface (Fig. 6b), and in a longitudinal direction along the windside centerline (Fig. 6c). Comparisons along the wing leading edge show differences that are generally less than 10%.

Even in the case where significant turning of streamlines occurs for flow expanding around the side of the vehicle ($32 < j < 48$), in Fig. 5a the integral-boundary-layer extrapolation from the baseline CFD computation is an excellent predictor of the CFD result at the off-baseline catalysis model. Though not shown in the figures, the method 1G predictions for a noncatalytic surface using either the fully catalytic baseline or the finite catalytic baseline also agree within a few percent.

The results in Figs. 5 and 6 do not include the correction for dissociation-dominated chemistry in the boundary layer as defined in Eq. (17). The correction was evaluated and found to represent less than 1% of the total heating along the windside centerline for this case. The term grew unreasonably large as the leeside was approached. It appears that the curve fits to tabulated data for the reaction integral[2] I_D are used outside their range of validity. It is expected that this term would be of greater significance if the vehicle were at a smaller angle of attack and more dissociation occurred within the boundary layer. The differences shown for this test case are thought to be small enough to be acceptable for preliminary TPS design purposes.

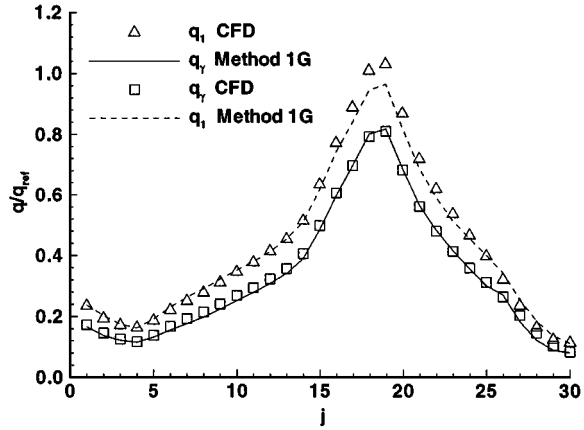

a) Wing, $i = 10$

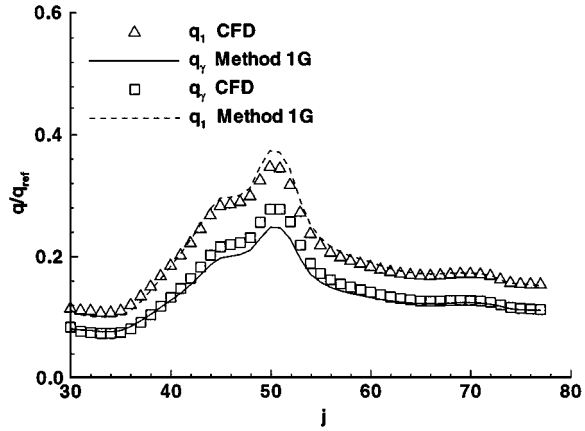

b) Windside, $i = 10$

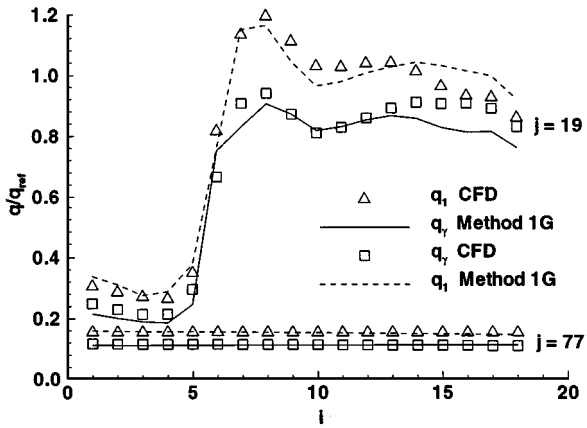

c) Centerline and wing leading edge, $j = 19, 77$

Fig. 6 Comparison of CFD heating levels obtained on midsection of RLV with method 1G predictions obtained at $\gamma = \gamma(T)$ and 1 at Mach 25 and 79.6 km.

Concluding Remarks

A new approach for combining the insight afforded by integral boundary-layer analysis with comprehensive (but time-intensive) CFD flowfield solutions of the thin-layer Navier–Stokes equations is presented. It allows a designer at a workstation to determine how heat transfer rates and radiative equilibrium wall temperatures change as a function of changes to surface catalytic efficiencies and emissivities. The approach extracts CFD-derived quantities at the wall and at the boundary-layer edge for inclusion in a postprocessing boundary-layer analysis, valid for most of the acreage on a realistic hypersonic vehicle.

In its original formulation, method 1 utilized limiting forms of boundary-layer parameters valid in the stagnation region to compute changes to surface heating associated with changes in surface catalysis. Method 1 proved the viability of this approach to engineering

design using a single CFD baseline solution but was not generally applicable to complex configurations. Method 1G is a straightforward extension of method 1 that is applicable to the entire vehicle. Rather than employing limiting forms of the boundary-layer equations or integrating along streamlines, it solves for an integral-boundary-layer streamline parameter to match the local CFD baseline heating rate. This parameter is then used to predict heating rates at off-baseline values of surface catalysis. Off-baseline predictions of heating rates by method 1G were generally in very good agreement with CFD solutions.

Some additional tuning of the method may still be required as the role of nitrogen atoms predominates the role of oxygen atoms in the diffusional component of catalytic heating. Also, the consistency of these predictions over a broader range of entry conditions and geometric complexity remains to be established before method 1G (or a related approach) can be used with confidence in a design mode. The calculations presented here using method 1G offer strong evidence that this design goal is within reach.

It is advised that fully catalytic baseline CFD solutions be run early in the design phase of a hypersonic vehicle. This approach yields CFD solutions for laminar, nonequilibrium flows that 1) are conservative, 2) converge more quickly than with finite catalytic or noncatalytic surface conditions, and 3) provide the best baseline for analytic extrapolation to various TPS design options.

References

[1]Inger, G. R., and Gnoffo, P. A., "Hypersonic Entry Heating with Discontinuous Surface Catalycity: A Combined Analytic/CFD Approach," AIAA Paper 96-2150, June 1996.

[2]Inger, G. R., "Nonequilibrium Boundary Layer Effects on the Aerodynamic Heating of Hypersonic Waverider Vehicles," *Journal of Thermophysics and Heat Transfer*, Vol. 9, No. 4, 1995, pp. 595–604.

[3]Inger, G. R., "Nonequilibrium Stagnation Point Boundary Layers with Arbitrary Surface Catalycity," *AIAA Journal*, Vol. 1, No. 8, 1963, pp. 1776–1784.

[4]Inger, G. R., and Elder, J., "Recombination Dominated Nonequilibrium Heat Transfer to Arbitrarily Catalytic Hypersonic Vehicles," *Journal of Thermophysics and Heat Transfer*, Vol. 5, No. 4, 1992, pp. 449–455.

[5]Gnoffo, P. A., and Inger, G. R., "Analytic Corrections to CFD Heating Predictions Accounting for Changes in Surface Catalysis," AIAA Paper 96-1800, June 1996.

[6]Gnoffo, P. A., "Point-Implicit Relaxation Strategies for Viscous, Hypersonic Flows," *Computational Methods in Hypersonic Aerodynamics*, edited by T. K. S. Murthy, Kluwer Academic, Norwell, MA, 1991, pp. 115–151.

[7]Gnoffo, P. A., "Upwind-Biased, Point-Implicit Relaxation Strategies for Viscous, Hypersonic Flows," AIAA Paper 89-1972, June 1989.

[8]Gnoffo, P. A., "An Upwind-Biased, Point-Implicit Relaxation Algorithm for Viscous, Compressible Perfect-Gas Flows," NASA TP-2953, Feb. 1990.

[9]Gnoffo, P. A., "Code Calibration Program in Support of the Aeroassist Flight Experiment," *Journal of Spacecraft and Rockets*, Vol. 27, No. 2, 1990, pp. 131–142.

[10]Weilmuenster, K. J., and Gnoffo, P. A., "Aeroassisted Flight Experiment Aerodynamic Characteristics at Flight Conditions," *Journal of Spacecraft and Rockets*, Vol. 27, No. 6, 1990, pp. 684–686.

[11]Thompson, R. A., and Gnoffo, P. A., "Application of the LAURA Code for Slender Vehicle Aerothermodynamics," *Journal of Spacecraft and Rockets*, Vol. 29, No. 1, 1992, pp. 16–23.

[12]Weilmuenster, K. J., Gnoffo, P. A., and Greene, F. A., "Navier–Stokes Simulations of Orbiter Aerodynamic Characteristics Including Pitch Trim and Bodyflap," *Journal of Spacecraft and Rockets*, Vol. 31, No. 3, 1994, pp. 355–366.

[13]Gnoffo, P. A., Weilmuenster, K. J., and Alter, S. J., "Multiblock Analysis for Shuttle Orbiter Re-entry Heating from Mach 24 to Mach 12," *Journal of Spacecraft and Rockets*, Vol. 31, No. 3, 1994, pp. 367–377.

[14]Roe, P. L., "Approximate Riemann Solvers, Parameter Vectors, and Difference Schemes," *Journal of Computational Physics*, Vol. 43, Oct. 1981, pp. 357–372.

[15]Harten, A., "High Resolution Schemes for Hyperbolic Conservation Laws," *Journal of Computational Physics*, Vol. 49, No. 2, 1983, pp. 357–393.

[16]Yee, H. C., "On Symmetric and Upwind TVD Schemes," NASA TM-88325, June 1986.

[17]Stewart, D. A., Leiser, D. B., Kolodziej, P., and Smith, M., "Thermal Response of Integral Multicomponent Composite Thermal Protection Systems," AIAA Paper 85-1056, June 1985.

[18]Stewart, D. A., "Surface Catalysis and Characterization of Proposed Candidate TPS for Access-to-Space Vehicles," NASA TM-112206, July 1997.

[19]Goulard, R. J., "On Catalytic Recombination Rates in Hypersonic Stagnation Heat Transfer," *Jet Propulsion*, Vol. 28, No. 11, 1958, pp. 737–745.

T. C. Lin
Associate Editor